TÜBİTAK

Turkish Journal of Earth Sciences

http://journals.tubitak.gov.tr/earth/

Research Article

Turkish J Earth Sci
(2021) 30: 235-246

doi:10.3906/yer-2011-18

Active tectonic stress field analysis in NW Iran-SE Turkey using earthquake focal mechanism data

Ahad NOURI MOKHOORI[1,*], Behnam RAHIMI[1], Mohsen MOAYYED[2]

[1] Department of Geology, Faculty of Sciences, Ferdowsi University of Mashhad, Mashhad, Iran

[2] Department of Geology, Faculty of Natural Sciences, University of Tabriz, Tabriz, Iran

Received: 19.11.2020 • **Accepted/Published Online:** 04.03.2021 • **Final Version:** 22.03.2021

Abstract: NW Iran-SE Turkey is a tectonically active zone related to the Arabia-Eurasia convergence, but the active stress state in this zone has not yet been clearly studied. To improve the knowledge of present-day stress state in this region, optimum reduced stress tensor was analysed. For this, a large number of earthquake focal mechanisms (277) were collected. The analyses show most mechanisms exhibit strike-slip to thrust faulting. These data indicate that this region is dominated by an N158° maximum horizontal compressive stress (S_{Hmax}) belonging to a transpressional tectonic regime. In the scale of the study area, the relative magnitude of the intermediate and minimum principal stress axes do not differ much ($\phi = 0.09$). Brittle deformation in this area is dominantly accommodated by a combination of strike-slip and thrust faulting ($A\phi = 1.82$ to 2.30). The analyses reveal that two sets of faults show a high tendency to slip and reactivate. These sets contain NW-SE-striking right-lateral and NNE-SSW-striking left-lateral faults. The results of this study may help to study the active seismicity, tectonic activity, and seismic risk in this region.

Key words: Stress inversion, stress regime, focal mechanism solution, active tectonic, NW Iran-SE Turkey

1. Introduction

In recent decades, present-day crustal stress state has been the subject of several studies (e.g., Delvaux and Barth, 2010; Hardebeck and Okada, 2018; Heidbach et al., 2018). Earthquakes in the crust are concerned with slip along fault surface in relation to the stresses acting on. The studies on P-wave first-motion polarities of the earthquakes reveal geometry and mechanism of faulting (Hardebeck and Shearer, 2002). Hence, earthquake focal mechanisms are the major database in active stress state analysis (e.g., Heidbach et al., 2018; Hardebeck and Okada, 2018). To reconstruct the present-day stress field from earthquake focal mechanisms, some inversion methods have been developed (e.g., Angelier, 2002; Delvaux and Barth, 2010). With the assumption that the stress state is uniform in time and space, and also faults slip parallel to maximum shear stress (Wallace, 1951), the methods try to minimize the angular difference between the observed and theoretically modelled slip direction, α (Angelier, 2002). The results are defined by four parameters: σ_1, σ_2, σ_3, and stress ratio ϕ, as defined by Angelier (2002), $\phi = (\sigma_2 - \sigma_3)/(\sigma_1 - \sigma_3)$.

Knowledge of stress state is an essential prerequisite for (i) describing deformation style and geodynamic of an area (Heidbach et al., 2018), (ii) discussing on rupture path, its propagation and associated earthquakes (Hardebeck and Okada, 2018), (iii) explaining faulting pattern in different areas of a region (Simpson, 1997), and (iv) evaluating slip and reactivation tendency of a fault (Lisle and Srivastava, 2004; Leclère and Fabbri, 2013).

To aid in the enhancement of knowledge in the tectonic regime of the NW Iran-SE Turkey, present-day active stress field was determined. To better understand the kinematic and faulting features of this region, results were combined with previous studies and discussed.

2. Regional structure and active deformation

Present-day structural framework of the Iranian-Turkish plateau and adjacent area is connected to the collisional evolution of the Arabian-Eurasian plates since Late Cretaceous-Early Palaeocene time (Berberian and King, 1981). Bitlis-Zagros thrust fault zone specifies the associated suture zone. However, the timing of the collision is a point not agreed upon. The collision develops a compressional stress regime and consequently, this regime mostly changed to strike-slip one. Development of the strike-slip system has been probably dominant since Miocene time (Allen et al., 2004).

Present-day convergence between the Arabian (in the south) and the Eurasian (in the north) plates determined 20 to 30 mm/year (Reilinger et al., 2006). This rate toward

* Correspondence: ahad.nouri@mail.um.ac.ir

NW Iran-SE Turkey decreases to ~13 mm/year (Reilinger et al., 2006). The convergence is partitioned into right-lateral movements in NW Iran-SE Turkey and thrusting in the Greater Caucasus (Jackson, 1992). Northward motion of the Arabian plate enforces westward escape of the Anatolian block along the North and East Anatolian faults (Allen et al., 2006) and N-S shortening in the Caucasus (Jackson, 1992; Copley and Jackson, 2006). NW Iran is a portion of this tectonically active region sandwiched between the Zagros Mountains in the south, the Caucasus in the north, and the Caspian block in the east. The related active deformation in this area is reflected in active faulting, folding, seismicity, and Quaternary volcanoes (Berberian, 1997, 1994; Dhont and Chorowicz, 2006).

The study area is located between the Pambak-Sevan-Sunik fault in the north, the Talesh fault zone in the east, the Çobandede fault zone in the west, and the Bitlis-Zagros fault in the south (Figure 1). In a general view, the study area comprises different types of active faults: NW-SE-striking right-lateral faults as major fault set have got more attention (e.g., North Tabriz fault) (Berberian, 1997; Faridi et al., 2017) and associated NNE-SSW-striking left-lateral conjugate faults (e.g., Aras fault) (Faridi et al., 2017), ~E-W-striking thrust faults mainly accommodated in the Transcaucasian region (Berberian, 1997), and ~NNW-SSE-striking normal faults (e.g., Serow fault) (Karakhanian et al., 2004).

In this region, most of the deformation accommodates along the faults (Jackson et al., 1995; Djamour et al., 2011). In this framework, seismic slip along the NW-SE-striking right-lateral faults are noticeable (Berberian, 1997). The strike-slip faulting fade toward north, as in Caucasus, thrust faulting is dominant (Jackson, 1992; Jackson et al., 1995).

3. Data and methodology

To compute the optimum stress tensor using earthquake focal mechanisms, 277 mechanisms were collected from various sources, including Jackson et al. (1995), Mostriouk and Petrov (1994), Bernardi et al. (2004), Pinar et al. (2007), Siahkali Moradi et al. (2009, 2011), Irmak et al. (2012), Görgün (2013), Nemati (2013), Kalafat et al. (2014), Ansari et al. (2015), Donner et al. (2015), Tseng et al. (2016), Afra et al. (2017), Momeni and Tatar (2018), Solaymani-Azad et al. (2019), Hosseini et al. (2019), Lukk and Shevchenko (2019), Global Centroid Moment Tensor (GCMT), Kandilli Observatory and Earthquake Research Institute (KOERI), International Seismological Centre (ISC), and United States Geological Survey (USGS). One difficulty concerning the gathered data set is the different focal mechanism solutions reported for the same event. In this case, a well-constrained report which was more compatible with the computed stress tensor was selected. Type of the focal mechanisms determined using the Frohlich triangle diagram (Frohlich, 1992) (Figures 2 and 3a).

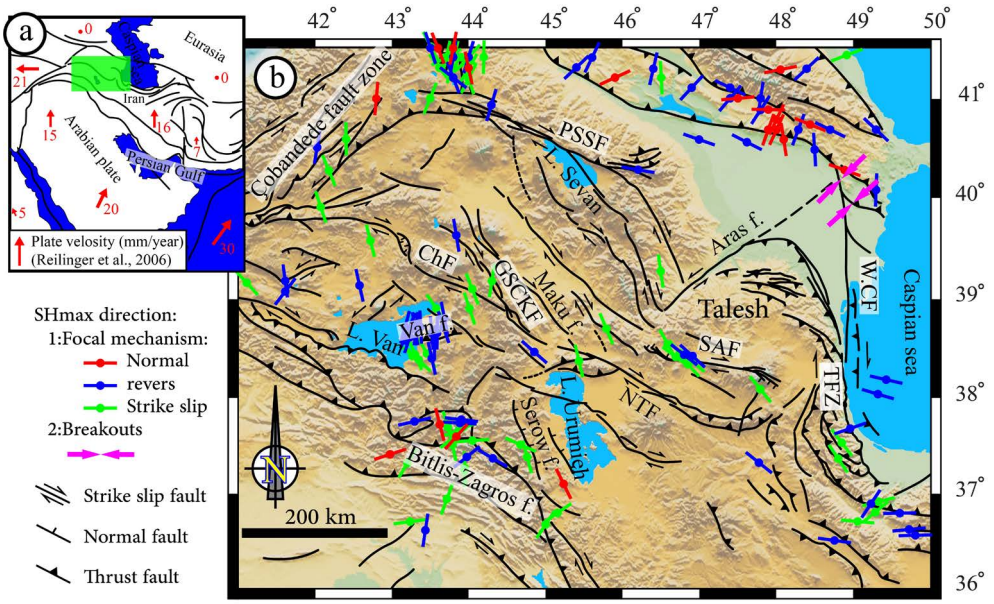

Figure 1. General tectonic map of the NW Iran-SE Turkey and adjacent areas. (a) The location of the study area (colored as green rectangle) in the Arabia-Eurasia collision zone (Baniadam et al., 2019). (b) The major active faults map of the NW Iran-SE Turkey prepared based on Karakhanian et al. (2004), Dhont and Chorowicz (2006), Aziz Zanjani et al. (2013), and Faridi et al. (2017). ChF: Çaldıran fault, GSCKF: Gailatu-Siah Cheshmeh-Khoy fault, NTF: North Tabriz fault, PSSF: Pambak-Sevan-Sunik fault, SAF: South Ahar fault, TFZ: Talesh fault zone and WCF: West Caspian fault. S_{Hmax} axes are from the World Stress Map (Heidbach et al., 2018).

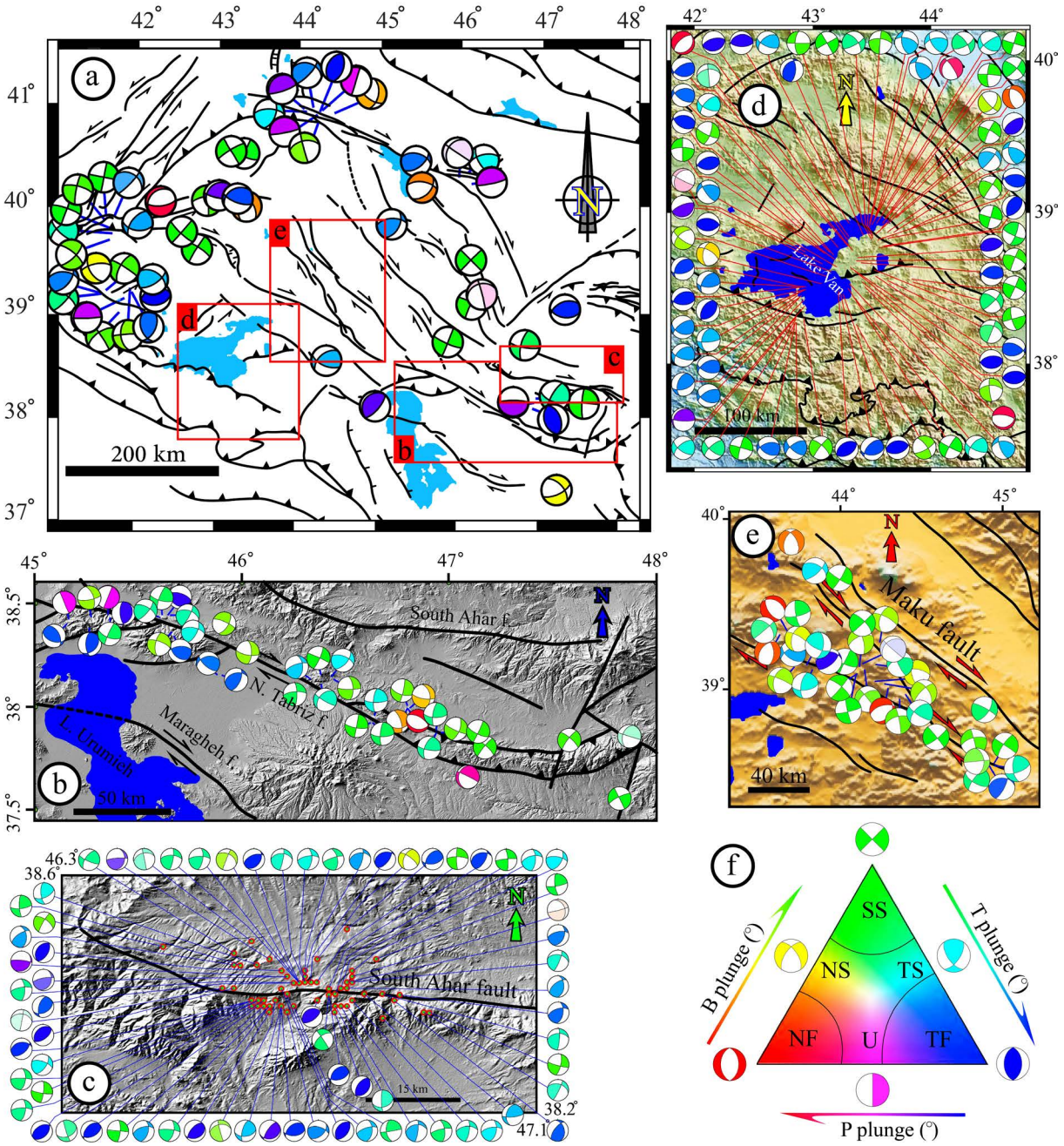

Figure 2. Earthquake focal mechanisms used to compute stress state. (a) represents the mechanisms used to estimate the regional stress state together with mechanisms in (b), (c), (d), and (e). (b), (c), (d), and (e) show mechanisms used to reconstruct the state of stress along the NTF, SAF, Van fault, and GSCKF, respectively. The color of focal mechanisms indicates their types based on the Frohlich triangle diagram (Frohlich, 1992), (f) Frohlich diagram modified by Soumaya et al. (2015) and this study. SS: strike-slip, TF: thrust, U: unknown, NF: normal, TS: thrust to strike-slip, and NS: normal to strike-slip faulting type.

Inversion of focal mechanisms solutions was performed using the method proposed by Delvaux and Barth (2010), which is implemented in the WINTENSOR software (Delvaux and Sperner, 2003) (version 5.8.9, 2019/09/05). To select the preferred seismic fault planes as the actual plane from the auxiliary one, we use the misfit function (F5) value, as defined by Delvaux and Barth (2010). F5 value shows facility of slip on fault planes under

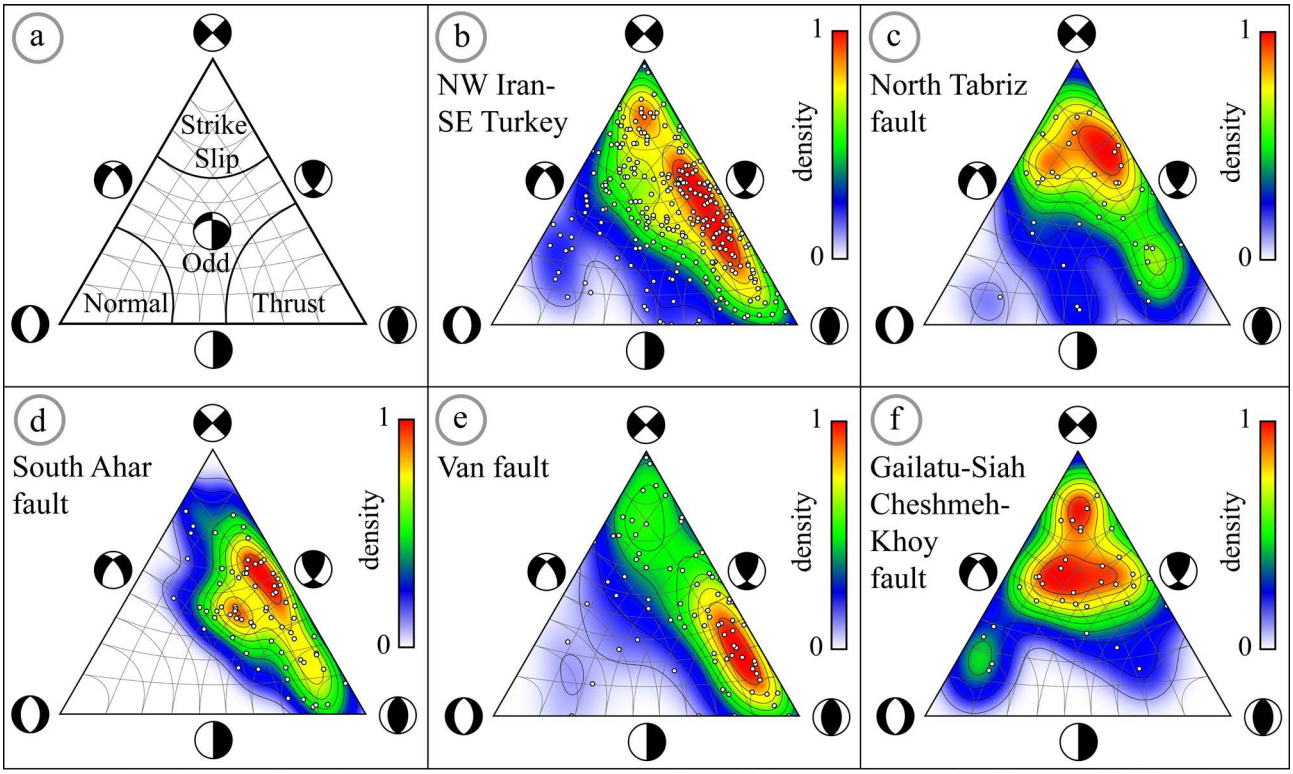

Figure 3. Definition of the different faulting types on the Frohlich diagram (a) and contoured triangle diagram plots of the earthquake focal mechanisms used to analyse the stress field in NW Iran-SE Turkey (b) and along the NTF (c), SAF (d), Van fault (e), and GSCKF (f), respectively.

the given stress field by 1: maximizing the resolved shear stress magnitude in order to favour slip and 2: minimizing the resolved normal stress magnitude in order to reduce the friction on the given plane. The value is independent from the ratio σ_1/σ_3 and ranges from 0 for the perfect fault plane as a more potential plane for shearing to 360 for the perfect misfit plane as a more stable plane. For reliable inversion results, we computed the stress tensor by at least 30 focal mechanisms (Hardebeck and Michael, 2006). The orientation of the maximum horizontal compressive stress (S_{Hmax}) was estimated following Lund and Townend (2007) and stress regime determined based on Ritz and Taboada (1993). To define the deformation type, we utilize the Aϕ parameter (Simpson, 1997). Aϕ values vary smoothly from 0 (radial normal faulting) to 1.5 (strike-slip faulting) and 3 (radial reverse faulting). The Index Aϕ is defined numerically as follows:

$$A\phi = (n + 0.5) + (-1)^n (\phi - 0.5) \quad (1)$$

Where, ϕ is the shape ratio of the stress state and n is 0 for normal, 1 for strike-slip, and 2 for reverse faulting.

Finally, we use the normalized slip tendency (Lisle and Srivastava, 2004) and 3-D reactivation (Leclère and Fabbri, 2013) analysis to test instability of the selected fault planes, which are the base of our proposed kinematic model.

4. Results

Considering the stress state is a fundamental control on reactivation of preexisting faults (Lisle and Srivastava, 2004; Leclère and Fabbri, 2013), stress state analysis was carried out in both regional and local (along-fault) scales.

4.1. Regional stress state

The focal mechanisms along the four selected faults were used to compute the regional stress state together with those located outside the four fault zones (Figure 2). The 277 mechanisms mostly show thrust to strike-slip faulting (Figure 3b). The reduced stress tensor that was computed on all 277 selected nodal planes (Figure 4) is compatible with a transpressional stress tensor with an N158° (1σ = 7.9°) directed S_{Hmax}. Estimated Aϕ equals 2.09, which shows mixing of reverse and strike-slip faulting (Table).

4.2. Local (along-fault) stress state

4.2.1. North Tabriz fault (NTF)

Seismically active right-lateral strike-slip NTF is a clear NW-SE-trending tectonic structure with a roughly vertical trace in the north of Tabriz city (Solaymani-Azad et al., 2015). GPS measurements indicate 7 ± 1 mm/year right-lateral motion, which takes place along the NTF (Djamour et al., 2011). Neotectonic activity along this fault is high-

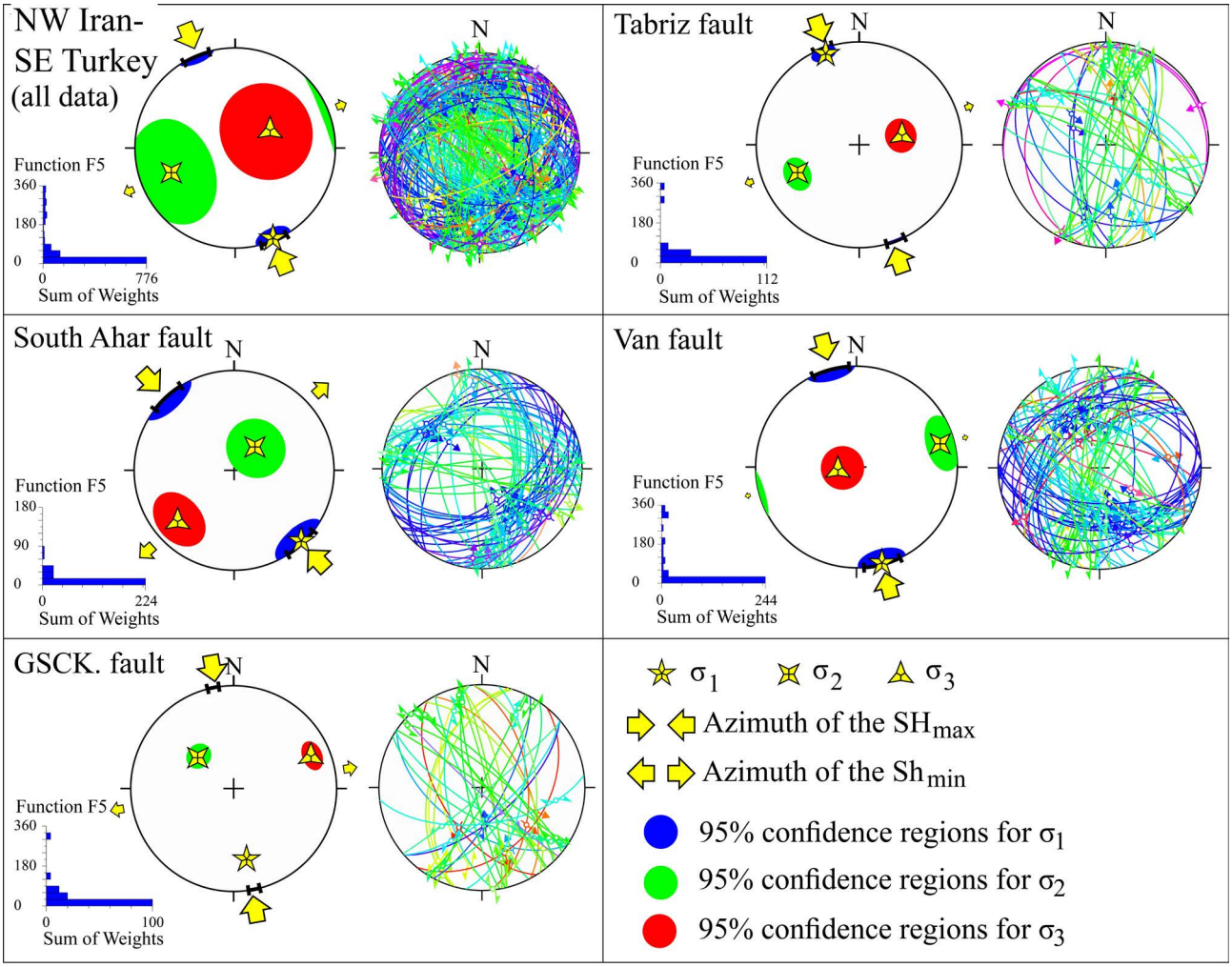

Figure 4. Stress inversion results (left) and stereoplot of the selected nodal planes (right) on the lower hemisphere equal-area projection for NW Iran-SE Turkey and NTF, SAF, Van fault, and GSCKF. Lengths of the maximum (S_{Hmax}) and minimum (S_{hmin}) horizontal stress are relative to the isotropic stress.

lighted by right-lateral displacements, historical earthquakes, and microseismicity (Berberian, 1994, 1997; Siahkali Moradi et al., 2011; Solaymani-Azad et al., 2015).

The earthquake focal mechanisms used to construct the on-going stress field on the NTF mostly show strike-slip to thrust faulting features (Figures 2b and 3c). Stress state along this fault (Figure 4) is described by a transpressional stress tensor. S_{Hmax} is directed in N161° with a small dispersion (1σ = 5.3°) fitting well to the selected fault planes (Table).

4.2.2. South Ahar fault (SAF)

Roughly E-W-striking SAF, sometimes known as Qoshadagh fault (Faridi et al., 2019), lies in the south of Ahar city. The SAF is characterized by right-lateral strike-slip movements with a component of thrust motion (Copley et al., 2013). The fault probably is the southeastern prolongation of the Nakhchivan fault (Faridi et al., 2019). This fault is the cause of the 2012 August 11 Ahar-Varzegan earthquakes (Mw 6.4 at 12:23 UTC and Mw 6.3 at 12:34 UTC). Indeed, the SAF is previously unknown and the earthquakes have led it to get attention as an active fault (Copley et al., 2013; Donner et al., 2015; Ghods et al., 2015). The slip at a rate of 1.9 ± 0.1 mm/year along it (Faridi et al., 2019) has right-laterally produced ≈2 km displacement in channels (Donner et al., 2015).

The focal mechanisms (70) were reported along the SAF characterized by a combination of strike-slip and thrusting types. (Figures 2c and 3d). These mechanisms describe a stress tensor belonging to a transpressional tectonic regime. This stress tensor affects the SAF by an NW-SE-trending S_{Hmax} (137°, 1σ = 10.1°) (Figure 4, Table).

Table. Parameters of the stress tensors. NTF, SAF, and GSCKF refer to North Tabriz, South Ahar, and Gailatu-Siah Cheshmeh-Khoy faults, respectively.

Name	n	σ_1	σ_2	σ_3	ϕ	α	$A\phi$	S_{Hmax}	1σ	DT
All data	277	03/158	32/249	58/063	0.09	32.7	2.09	158	7.9	RS
NTF	40	06/340	34/246	55/079	0.19	27	2.19	161	5.3	RS
SAF	70	03/137	65/041	25/228	0.18	14.7	1.82	137	10.1	SR
Van f.	79	02/165	15/075	75/261	0.3	30	2.3	164	10.1	R
GSCKF	35	31/170	52/310	20/068	0.02	25.2	1.98	170	3.2	SR

n: number of the nodal planes used in the stress inversion, σ_1, σ_2, and σ_3: orientation of the principal stress axes given as plunge/trend, ϕ: stress ratio, α: misfit angle, $A\phi$: faulting type index, S_{Hmax}: orientation of the maximum horizontal stress axis, 1σ: standard deviation and DT: deformation type, RS: reverse with strike-slip, SR: strike-slip with reverse, R: reverse.

4.2.3. Van fault

Van basin has been regarded as a ramp basin of the compressional Bitlis-Zagros belt that its active tectonic is highlighted by Plio-Quaternary volcanoes associated with roughly N-S trending fissures (Dhont and Chorowicz, 2006). Both roughly northward motion of the Arabian plate and westward escape of the Anatolian block affect this area (Allen et al., 2006; Dhont and Chorowicz, 2006). The Van fault is a north dipping blind-oblique-slip fault with predominant thrust movement (Akoğlu et al., 2018). Right-lateral movements from 8 ± 2 mm/year along the Çaldıran fault decrease to 2–3 mm/year in the south of the Lake Van (Copley and Jackson, 2006).

Selected focal mechanisms along the Van fault zone mostly show thrust to strike-slip faulting (Figures 2d and 3e). Computed stress tensor acts as compressional stress. The optimum reduced stress tensor is characterized by an N165° (1σ = 10.1°) S_{Hmax} acting roughly perpendicular on the Van fault (Figure 4, Table).

4.2.4. Gailatu-Siah Cheshmeh-Khoy fault (GSCKF)

The active NW-SE-trending right-lateral strike-slip GSCKF probably is the northwestern termination of the NTF (Berberian, 1997; Karakhanian et al., 2004; Siahkali Moradi et al., 2011). Right-lateral movements along this fault take place at a rate of ~8 mm/year (Selçuk et al., 2016). The NTF in contribution with the GSCKF plays a key role in transferring the right-lateral movements from NW Iran toward SE Turkey (Djamour et al., 2011). Toward north, active WNW-ESE-striking Çaldıran fault branches from the GSCKF (Selçuk et al., 2016; Berberian, 1997).

Selected 35 focal mechanisms for simulating the stress state along the GSCKF mostly show strike-slip and oblique-slip faulting (Figures 2e and 3f). These mechanisms explain a transpressional stress tensor with a well-constrained (1σ = 3.2°) N170° S_{Hmax} fitting well to the fault planes.

5. Discussion

5.1. Compatibility of the inferred stress state with the structural framework

The geological and geomorphological evidence, source parameters of large magnitude earthquakes, and GPS measurements indicated deformation in the NW Iran-SE Turkey mostly accommodate by oblique-slip movements along the discontinuous faults (Karakhanian et al., 2004; Copley and Jackson, 2006; Reilinger et al., 2006; Djamour et al., 2011; Solaymani-Azad et al., 2015, 2019). That the activity of the region is resulted from the convergence between the Arabian and Eurasian plates is an accepted fact (Jackson, 1992; Allen et al., 2006, 2004; Reilinger et al., 2006; Djamour et al., 2011).

Based on the inversion of earthquake focal mechanisms, in the regional scale, the dominant stress state estimated from 277 focal mechanisms enforces this area to activity by an N158° S_{Hmax}. The direction of the S_{Hmax} is in line with the moving direction of the plates affecting the area (Reilinger et al., 2006; Djamour et al., 2011) and kinematic of the well-known faults, such as NTF, GSCK, and Çaldıran faults, as well (Karakhanian et al., 2004; Copley et al., 2013; Faridi et al., 2019, 2017; Solaymani-Azad et al., 2019, 2015) .

NTF is affected by a transpressional stress regime. Value of the index $A\phi$ (2.19) shows deformation along the NTF accommodates by thrusting with strike-slip faulting. Some studies point out folds that developed roughly parallel to the NTF (Nouri Mokhoori, 2013; Mesbahi et al., 2016). These show both ductile and brittle contractional structures have been accommodated a part of the on-going deformation.

According to the extensional structures developed in Tabriz city, Karakhanian et al. (2004) concluded that Tabriz city (in the southern side of NTF) is located in an active pull-apart basin. Ahmadzadeh et al. (2014)

believed the structures are developed in the Miocene to Plio-Quaternary sedimentary units. According to Faridi and Khodabandeh (2012), these units are covered by the younger ones without any extension structures. Besides, studies on the seismotectonic of the NTF show there is no seismic evidence of extension (Siahkali Moradi et al., 2011). Therefore, it can be concluded that the pull-apart associated extension in the Tabriz area (Karakhanian et al., 2004) is not active now.

The activity of the SAF derives from N137° S_{Hmax}. Considering S_{Hmax} direction relative to the SAF, oblique-slip movement is expected for this fault. Right-lateral movements are highlighted by right-lateral offsets (Donner et al., 2015) and transtensional horsetail structures splaying from terminations of this fault (Faridi et al., 2019). Structural studies on the Quaternary units adjacent to this fault (Ghods et al., 2015) show roughly ESE-WNW-trending contractional structures are developed. These structures can accommodate a portion of the compressional component of the on-going deformational phase.

Based on the estimated stress tensor, the Van fault zone is dominated by N164° S_{Hmax}, roughly perpendicular to the Van fault zone. This orientation enforces this fault zone to dominant thrust faulting ($A\phi = 2.30$). Dhont and Chorowicz (2006) showed several Quaternary volcanoes aligned with roughly N-S orientation. The estimated stress state is consistent with roughly N-S fissures. However, Dhont and Chorowicz (2006) linked them to ~E-W-trending extension resulted from the westward escape of the Anatolian block (Allen et al., 2006).

Stress state around the GSCKF is characterized by a roughly N-S-oriented S_{Hmax} (N170°) belonging to a transpressional tectonic regime. GSCK fault is a right-lateral structure with an NNW-SSE-oriented strike. Northwestern termination of this fault forms horsetail structures containing a number of normal faults (Karakhanian et al., 2004). Indeed GSCKF contains a series of right-lateral faults. Right-lateral movements associated pull-apart basins along these faults are the remarkable feature of this fault (Karakhanian et al., 2004), which are highlighted in earthquake focal mechanisms (Figures 2e and 3f).

5.2. Kinematic model

Copley and Jackson (2006) proposed a simple model of fault and fault-bounded blocks rotation for kinematic of the central part of the study area. In this model, NW-SE-striking right-lateral PSSF, GSCKF, and Nakhichevan fault (NF) bounded two blocks. Left-lateral movements across the area on NE-SW planes enforce the faults and fault-bounded blocks to anticlockwise rotation (Figure 5a). This model reasonably explains slip sense along the block bounded faults, as well as slip rate along them (Copley and Jackson, 2006). In the study area, other three faults, namely Akhourian, Garni, and Maku faults, activate in a uniform sense and roughly parallel to PSSF, NF, and GSCKF (Figure 6a). We extend the model to the blocks bounded by these six NW-SE-striking right-lateral faults (Figure 6a). Sufficient evidences for rotation of a block can conclude by paleomagnetic and GPS studies. The paleomagnetic study carried out in the Van area (Gülyüz et al., 2020) is restricted to Miocene time, and therefore the results of this study cannot handle as evidence for active rotation of the area. Farther west, in the Sivas and Gümüşhane areas, as well as in Kırşehir block, paleomagnetic and GPS studies indicate

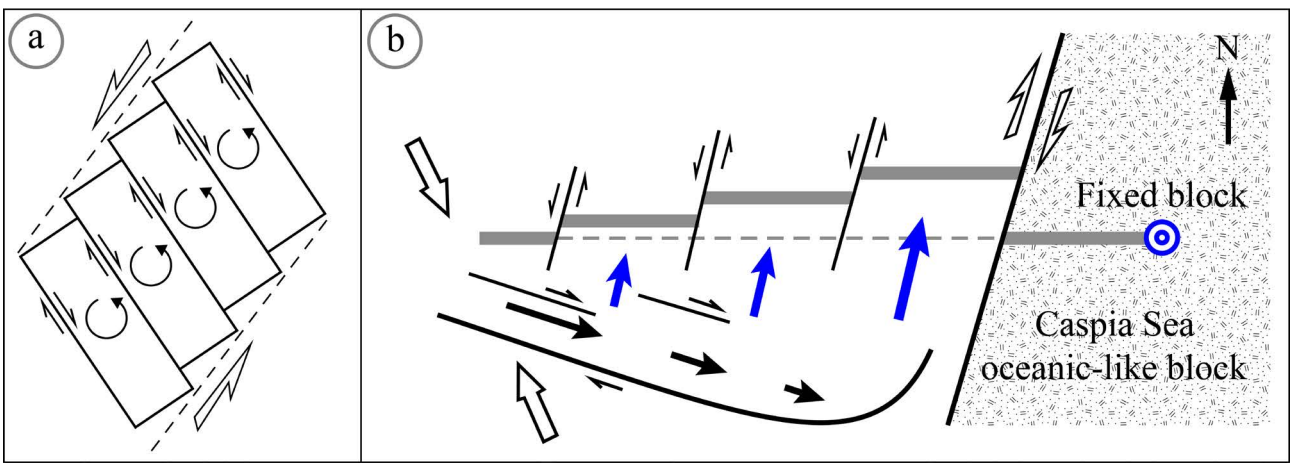

Figure 5. (a) A simplified model for kinematic of the central part of the study area containing NW-SE-striking PSSF, GSCKF, and NF (modified after Copley and Jackson (2006)). (b) Simplified kinematic model proposed for the area, especially SAF located in west of the Caspian Sea [modified after Ghods et al. (2015)]. Northward motion of the area relative to the South Caspian Basin cumulatively increases from west to east by displacement along the subsidiary NNE-SSW-striking left-lateral faults.

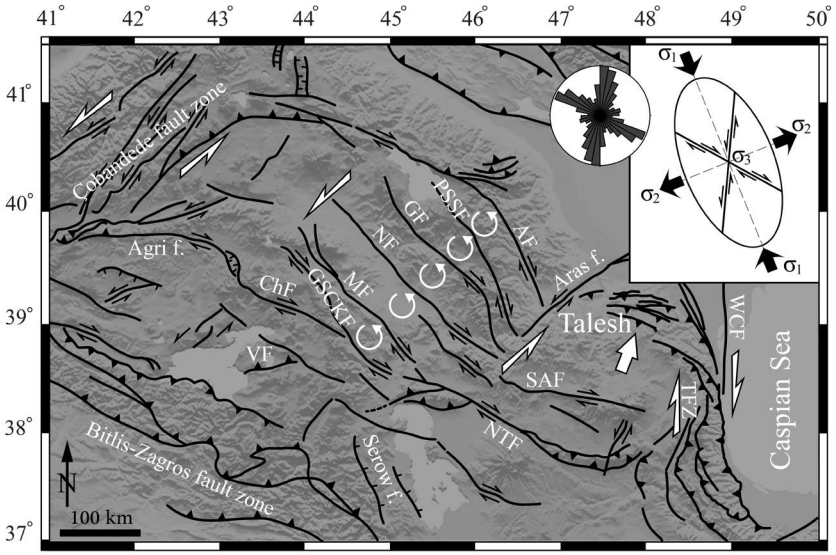

Figure 6. Simplified illustration of the present-day kinematic of the NW Iran-SE Turkey region. Bookshelf model and anticlockwise rotation of the blocks, which are bounded by AF, PSSF, GF, NF, MF, and GSCKF are presented. Considering the left-lateral movement of the NE-SW-striking Aras fault and right-lateral movement of the ~N-S-striking Talesh fault zone, NNW motion of the Talesh region located between these two fault zones, is expected. Inferred kinematic model from stress inversion is presented on the stress ellipsoid. Diameters of the stress ellipsoid are based on the relative magnitude of the maximum and minimum horizontal stress axes (Ritz and Taboada, 1993). Rose diagram shows two sets of faults which are highly instable. The NW-SE-striking right-lateral strike-slip and the NNE-SSW-striking left-lateral strike-slip faults are represented on the stress ellipsoid.

counterclockwise rotation of the region, which has taken place from Miocene (Kissel et al., 2003). Unfortunately, GPS network used to study the active deformation in NW Iran-SE Turkey is not dense enough to evaluate local deformation. GPS measurements show left-lateral shear through NE-SW-striking faults take place at the rate of ~8 mm/year [for detail, see Copley and Jackson (2006)] and active right-lateral movements along the NW-SE-striking faults are documented, as explained above.

Structural evolution and activity of the Talesh range are mainly affected by the rigid south Caspian block (SCB) (Berberian, 1983). Ghods et al. (2015) believed, rigidity of the SCB hampers eastward motion of the northern part of the SAF along this and other WNW to E–striking dextral faults. Therefore, all movement driven by large-scale plate motions cannot accommodate along these right-lateral faults. For accommodating of movements have remained, other structures, especially NNE-SSW-striking faults activate sinistrally (Figure 5b).

Considering the left-lateral slip sense of the NNE-SSW-striking Aras fault and right-lateral slip sense of the roughly N-S-striking Talesh fault zone located, respectively, in west and east of the Talesh, it can be expected that Talesh region experiences roughly NNE motion (Didon and Gemain, 1976) (Figure 6a), which is in agreement with plates motions (Reilinger et al., 2006).

The inferred stress state can be completely illustrated by a stress ellipsoid (Ritz and Taboada, 1993), as shown in Figure 6b. Stress state analysis highlights two dominant sets of faults. The first set contains NW-SE-striking right-lateral faults and the second one contains NNE-SSW-striking left-lateral faults (Figure 6b). To evaluate the instability of these faults, we test slip tendency (Lisle and Srivastava, 2004) and 3D reactivation potential (Leclère and Fabbri, 2013) of these faults. Assuming cohesion on the faults equals 0 and μ~0.6 (as typical value of Byerlee friction coefficient), most of the selected faults achieve a high slip tendency value (Figure 7a).

3D reactivation analysis distinguishes three classes of faults (Leclère and Fabbri, 2013): (i) favorably oriented faults are those, which show a high tendency to reactivate in the given stress field, (ii) unfavorably oriented faults are those, whose reactivation can be attained by one or combination of two mechanisms: magnitude of pore fluid

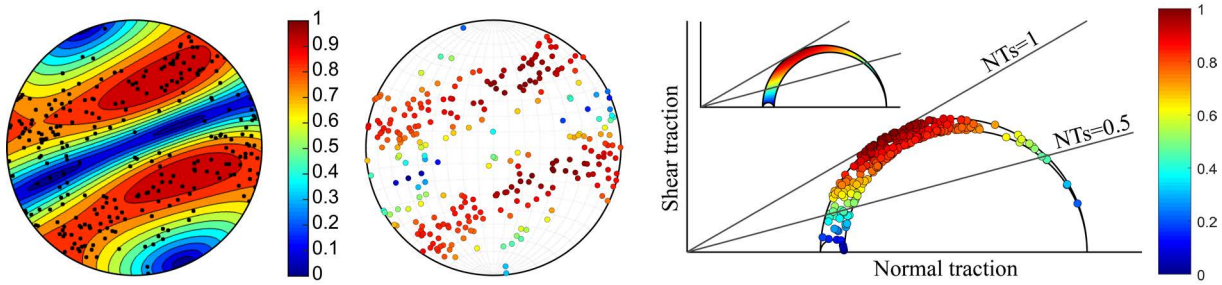

Figure 7. Stereographic and Mohr plot expression of the normalized slip tendency analysis integrated with poles to the selected fault planes.

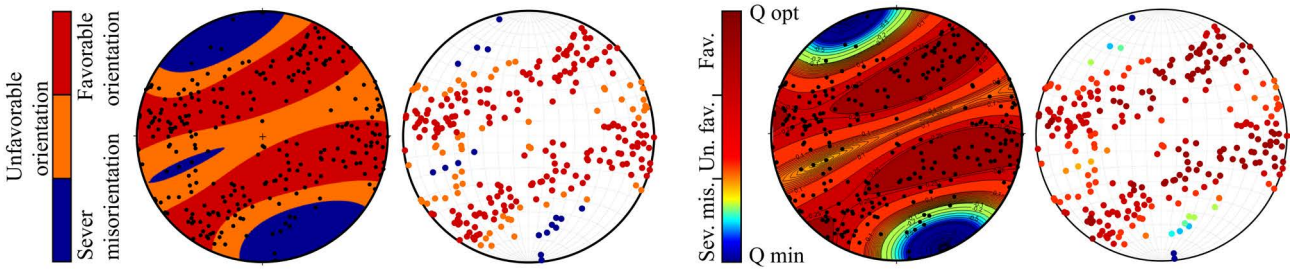

Figure 8. The results of the 3-D reactivation analysis. Stereoplot shows the three class of fault planes and stereographic expression of the contoured Q values. The side colored bar shows how prone the fault planes are to reactivation. Black dots represent the poles to the planes.

pressure remains higher than zero and lower than those of the minimum principal stress ($0 < p_f < \sigma_3$), or tectonic loading lead to an increase in the magnitude of the maximum principal stress, and (iii) severely misoriented faults are those, whose reactivation can only be attained if pore fluid pressure achieves a magnitude larger than those of the minimum principal stress ($p_f > \sigma_3$). (Leclère and Fabbri, 2013). 3D reactivation analysis under the same conditions to slip tendency analysis indicates most of the selected fault planes to analyse the stress state are favorably oriented with respect to the inferred stress field (Figure 8). As represented in Figure 6, we propose present-day deformation of the study area accommodates by these two sets of faults. These sets of unstable faults are in good agreement with field observations (Faridi et al., 2017).

6. Conclusion

As revealed by the result of the stress inversion using the 277 earthquake focal mechanisms, the regional stress state of the NW Iran-SE Turkey is characterized by a transpressional tectonic regime with N158° maximum horizontal compressive stress (SHmax). The stress inversion results in the regional scale show the relative magnitudes of the intermediate and minimum principal stresses are close to each other ($\phi = 0.09$), and therefore stress permutation between axes of σ_2 and σ_3 can take place. Present-day kinematic of the area is mostly summarized in NW-SE-striking right-lateral and NNE-SSW-striking left-lateral faulting.

Acknowledgment

We thank Dr. Markos D. Tranos from the Aristotle University of Thessaloniki and Jens-Erik Lund Snee from Stanford University for their suggestions. We extend our sincere gratitude to Dr. Jussi Mattila from the Geological Survey of Finland for providing the slip-tendency analysis code. Also, Dr. Henri Leclère from Université de Franche-Comté is sincerely thanked for providing the fault reactivation analysis code. We would like to thank three anonymous reviewers for their reviews and comments.

References

Afra M, Moradi A, Pakzad M (2017). Stress regimes in the northwest of Iran from stress inversion of earthquake focal mechanisms. Journal of Geodynamics 111: 50-60. doi: 10.1016/j.jog.2017.08.003

Ahmadzadeh E, Nazari H, Talebian M, Solaymani-Azad S, Faridi M (2014). Morphotectonics and Paleoseismology investigation on Sahlan Fault Fragment, NW segment of the North Tabriz Fault. Iranian Journal of Geology 31: 35-47 (in Persian).

Akoğlu AM, Jónsson S, Wang T, Çakır Z, Dogan, U et al. (2018). Evidence for tear faulting from new constraints of the 23 October 2011 M w 7.1 Van, Turkey, earthquake based on InSAR, GPS, coastal uplift, and field observations. Bulletin of the Seismological Society of America 108: 1929-1946. doi: 10.1785/0120170314

Allen M, Jackson J, Walker R (2004). Late Cenozoic reorganization of the Arabia-Eurasia collision and the comparison of short-term and long-term deformation rates. Tectonics 23. doi: 10.1029/2003tc001530

Allen MB, Blanc E, Walker R, Jackson J, Talebian M et al. (2006). Contrasting styles of convergence in the Arabia-Eurasia collision: why escape tectonics does not occur in Iran. Special Papers-Geologıcal Socıety of America 409: 579. doi: 10.1130/2006.2409(26)

Angelier J (2002). Inversion of earthquake focal mechanisms to obtain the seismotectonic stress IV—a new method free of choice among nodal planes. Geophysical Journal International 150: 588-609. doi: 10.1046/j.1365-246x.2002.01713.x

Ansari S, Yaminifard F, Tatar M (2015). Moment tensor solution of the Central-Western Alborz (Iran) earthquakes based on regional data. Quaterly Geosciences 24: 359-368 (in Persian with English abstract).

Aziz Zanjani A, Ghods A, Sobouti F, Bergman E, Mortezanejad G et al. (2013). Seismicity in the western coast of the South Caspian Basin and the Talesh Mountains. Geophysical Journal International 195: 799-814. doi: 10.1093/gji/ggt299

Baniadam F, Shabanian E, Bellier O (2019). The kinematics of the Dasht-e Bayaz earthquake fault during Pliocene-Quaternary: implications for the tectonics of eastern Central Iran. Tectonophysics 772: 228218. doi: 10.1016/j.tecto.2019.228218

Berberian M, King G (1981). Towards a paleogeography and tectonic evolution of Iran. Canadian Journal of Earth Sciences 18: 210-265. doi: 10.1139/e81-019

Berberian M (1983). The southern Caspian: a compressional depression floored by a trapped modified oceanic crust. Canadian Journal of Earth Sciences 20: 163-183. doi: 10.1139/e83-015

Berberian M (1994). Natural hazards and the first earthquake catalogue of Iran. A UNESCO/IIEES Project during the United Nations International Decade for Natural Disaster Reduction (IDNDR: 1900–2000). Tehran, Iran: International Institute of Earthquake Engineering and Seismology (IIEES), p. 603 (in English), p. 66 (in Persian).

Berberian M (1997). Seismic sources of the Transcaucasian historical earthquakes. In: Giardini D, Balassanian S (editors). Historical and Prehistorical Earthquakes in the Caucasus. NATO ASI Series. Dordrecht, Netherlands: Kluwer Academic Press, pp. 233-311.

Bernardi F, Braunmiller J, Kradolfer U, Giardini D (2004). Automatic regional moment tensor inversion in the European-Mediterranean region. Geophysical Journal International 157: 703-716. doi: 10.1111/j.1365-246x.2004.02215.x

Copley A, Jackson J (2006). Active tectonics of the Turkish-Iranian plateau. Tectonics 25. doi: 10.1029/2005tc001906

Copley A, Faridi M, Ghorashi M, Hollingsworth J, Jackson J (2013). The 2012 August 11 Ahar earthquakes: consequences for tectonics and earthquake hazard in the Turkish–Iranian Plateau. Geophysical Journal International 196: 15-21. doi: 10.1093/gji/ggt379

Delvaux D, Sperner B (2003). New aspects of tectonic stress inversion with reference to the TENSOR program. Geological Society London Special Publications 212: 75-100. doi: 10.1144/gsl.sp.2003.212.01.06

Delvaux D, Barth A (2010) African stress pattern from formal inversion of focal mechanism data. Tectonophysics 482: 105-128. doi: 10.1016/j.tecto.2009.05.009

Dhont D, Chorowicz J (2006). Review of the neotectonics of the Eastern Turkish–Armenian Plateau by geomorphic analysis of digital elevation model imagery. International Journal of Earth Sciences 95: 34-49. doi: 10.1007/s00531-005-0020-3

Didon J, Gemain YM (1976). Le Sabalan volcan plio-quaternaire de l'Azerbaidjan oriental (Iran): étude géologique et pétrographique de l'édifice et de son environnement régional. PhD, University of Grenoble, Grenoble, France (in French).

Djamour Y, Vernant P, Nankali HR, Tavakoli F (2011). NW Iran-eastern Turkey present-day kinematics: results from the Iranian permanent GPS network. Earth and Planetary Science Letters 307: 27-34. doi: 10.1016/j.epsl.2011.04.029

Donner S, Ghods A, Krüger F, Rößler D, Landgraf A et al. (2015). The Ahar-Varzeghan earthquake doublet (M w 6.4 and 6.2) of 11 August 2012: regional seismic moment tensors and a seismotectonic interpretation. Bulletin of the Seismological Society of America 105: 791-807. doi: 10.1785/0120140042

Faridi M, Khodabandeh A (2012). Tabriz Quadrangle: 1:25,000 Scale Geological Map. Tehran, Iran: Geological survey and mineral exploration of Iran Publications (in Persian and English).

Faridi M, Burg J-P, Nazari H, Talebian M, Ghorashi M (2017). Active faults pattern and interplay in the Azerbaijan region (NW Iran). Geotectonics 51: 428-437. doi: 10.1134/s0016852117040033

Faridi M, Nazari H, Burg J-P, Haghipour N, Talebian M et al. (2019). Structural characteristics paleoseismology and slip rate of the Qoshadagh fault, northwest of Iran. Geotectonics 53: 280-297. doi: 10.1134/s0016852119020031

Frohlich C (1992) Triangle diagrams: ternary graphs to display similarity and diversity of earthquake focal mechanisms. Physics of the Earth and Planetary Interiors 75: 193-198. doi: 10.1016/0031-9201(92)90130-n

Ghods A, Shabanian E, Bergman E, Faridi M, Donner S et al. (2015). The Varzaghan–Ahar, Iran, Earthquake Doublet (M w 6.4, 6.2): implications for the geodynamics of northwest Iran. Geophysical Journal International 203: 522-540. doi: 10.1093/gji/ggv306

Görgün E (2013). The 2011 October 23 M w 7.2 Van-Erciş Turkey earthquake and its aftershocks. Geophysical Journal International 195: 1052-1067. doi: 10.1093/gji/ggt264

Gülyüz E, Durak H, Özkaptan M, Krijgsman W (2020). Paleomagnetic constraints on the early Miocene closure of the southern NeoTethys (Van region; East Anatolia): Inferences for the timing of Eurasia Arabia collision. Global and Planetary Change 185: 103089. doi: 10.1016/j.gloplacha.2019.103089

Hardebeck JL, Shearer PM (2002). A new method for determining first-motion focal mechanisms. Bulletin of the Seismological Society of America 92: 2264-2276. doi: 10.1785/0120010200

Hardebeck JL, Michael AJ (2006). Damped regional-scale stress inversions: Methodology and examples for southern California and the Coalinga aftershock sequence. Journal of Geophysical Research: Solid Earth 111. doi: 10.1029/2005jb004144

Hardebeck JL , Okada T (2018). Temporal stress changes caused by earthquakes: a review. Journal of Geophysical Research: Solid Earth 123: 1350-1365. doi: 10.1002/2017jb014617

Heidbach O, Rajabi M, Cui X, Fuchs K, Müller B et al. (2018). The World Stress Map database release 2016: crustal stress pattern across scales. Tectonophysics 744: 484-498. doi: 10.1016/j.tecto.2018.07.007

Hosseini H, Pakzad M, Naserieh S (2019). Iranian regional centroid moment tensor catalog: solutions for 2012–2017. Physics of the Earth and Planetary Interiors 286: 29-41. doi: 10.1016/j.pepi.2018.11.001

Irmak TS, Doğan B, Karakaş A (2012). Source mechanism of the 23 October, 2011, Van (Turkey) earthquake (M w= 7.1) and aftershocks with its tectonic implications. Earth, Planets and Space 64: 991-1003. doi: 10.5047/eps.2012.05.002

Jackson J (1992). Partitioning of strike-slip and convergent motion between Eurasia and Arabia in eastern Turkey and the Caucasus. Journal of Geophysical Research: Solid Earth 97: 12471-12479. doi: 10.1029/92jb00944

Jackson J, Haines J, Holt W (1995). The accommodation of Arabia-Eurasia plate convergence in Iran. Journal of Geophysical Research: Solid Earth 100: 15205-15219. doi: 10.1029/95jb01294

Kalafat D, Kekovalı K, Akkoyunlu F, Ögütçü Z (2014). Source mechanism and stress analysis of 23 October 2011 Van Earthquake (Mw = 7.1) and aftershocks. Journal of seismology 18: 371-384. doi: 10.1007/s10950-013-9413-0

Karakhanian AS, Trifonov VG, Philip H, Avagyan A, Hessami K et al. (2004). Active faulting and natural hazards in Armenia, eastern Turkey and northwestern Iran. Tectonophysics 380: 189-219. doi: 10.1016/j.tecto.2003.09.020

Kissel C, Laj C, Poisson A, Görür N (2003). Paleomagnetic reconstruction of the Cenozoic evolution of the Eastern Mediterranean. Tectonophysics 362: 199-217. doi: 10.1016/s0040-1951(02)00638-8

Leclère H, Fabbri O (2013). A new three-dimensional method of fault reactivation analysis. Journal of structural Geology 48: 153-161. doi: 10.1016/j.jsg.2012.11.004

Lisle RJ, Srivastava DC (2004). Test of the frictional reactivation theory for faults and validity of fault-slip analysis. Geology 32: 569-572. doi: 10.1130/g20408.1

Lukk A, Shevchenko V (2019). Seismicity, tectonics, and GPS geodynamics of the Caucasus. Izvestiya, Physics of the Solid Earth 55: 626-648. doi: 10.1134/s1069351319040062

Lund B, Townend J (2007). Calculating horizontal stress orientations with full or partial knowledge of the tectonic stress tensor. Geophysical Journal International 170: 1328-1335. doi: 10.1111/j.1365-246x.2007.03468.x

Mesbahi F, Mohajjel M, Faridi M (2016). Neogene oblique convergence and strain partitioning along the North Tabriz Fault, NW Iran. Journal of Asian Earth Sciences 129: 191-205. doi: 10.1016/j.jseaes.2016.08.010

Momeni S, Tatar M (2018). Mainshocks/aftershocks study of the August 2012 earthquake doublet on Ahar-Varzaghan complex fault system (NW Iran). Physics of the Earth and Planetary Interiors 283: 67-81. doi: 10.1016/j.pepi.2018.08.001

Mostriouk A, Petrov V (1994). Catalogue of focal mechanisms of earthquakes 1964–1990. Moscow, Russia: Materials of the World Data Center, p. 87.

Nemati M (2013). Some aspects about seismology of 2012 August 11 Ahar-Vaezaghan (Azarbayjan, NW of Persia) earthquakes sequences. Journal of Sciences, Islamic Republic of Iran 24: 229-241.

Nouri Mokhoori A (2013). Study of structure and seismotectonic of North tabriz fault (from Bostanabad to Marand) and estimation of the third order tectonic stresses. M.Sc., University of Tabriz, Tabriz, Iran (in Persian).

Pinar A, Honkura Y, Kuge K, Matsushima M ,Sezgin N et al. (2007). Source mechanism of the 2000 November 15 Lake Van earthquake (M w = 5.6) in eastern Turkey and its seismotectonic implications. Geophysical Journal International 170: 749-763. doi: 10.1111/j.1365-246x.2007.03445.x

Reilinger R, McClusky S, Vernant P, Lawrence S, Ergintav S et al. (2006). GPS constraints on continental deformation in the Africa-Arabia-Eurasia continental collision zone and implications for the dynamics of plate interactions. Journal of Geophysical Research: Solid Earth 111. doi: 10.1007/978-94-011-5464-2_4

Ritz J-F, Taboada A (1993). Revolution stress ellipsoids in brittle tectonics resulting from an uncritical use of inverse methods. Bulletin de la Société Géologique de France 164: 519-531.

Selçuk AS, Erturaç MK, Nomade S (2016). Geology of the Çaldıran Fault, Eastern Turkey: age, slip rate and implications on the characteristic slip behaviour. Tectonophysics 680: 155-173. doi: 10.1016/j.tecto.2016.05.019

Siahkali Moradi A, Tatar M, Hatzfeld D, Paul A (2009). Crustal velocity model and fault mechanism of the Tabriz Strike-Slip Zone. Quaterly Geosciences 18: 140-153.

Siahkali Moradi A, Hatzfeld D, Tatar M (2011). Microseismicity and seismotectonics of the North Tabriz fault (Iran). Tectonophysics 506: 22-30. doi: 10.1016/j.tecto.2011.04.008

Simpson RW (1997). Quantifying Anderson's fault types. Journal of Geophysical Research: Solid Earth 102: 17909-17919. doi: 10.1029/97jb01274

Solaymani-Azad S, Philip H, Dominguez S, Hessami K, Shahpasandzadeh M et al. (2015). Paleoseismological and morphological evidence of slip rate variations along the North Tabriz fault (NW Iran). Tectonophysics 640: 20-38. doi: 10.1016/j.tecto.2014.11.010

Solaymani-Azad S, Nemati M, Abbassi M-R, Foroutan M, Hessami K Dominguez S et al. (2019). Active-couple indentation in geodynamics of NNW Iran: evidence from synchronous left- and right-lateral co-linear seismogenic faults in western Alborz and Iranian Azerbaijan domains. Tectonophysics 754: 1-17. doi: 10.1016/j.tecto.2019.01.013

Soumaya A, Ben Ayed N, Delvaux D, Ghanmi M (2015). Spatial variation of present-day stress field and tectonic regime in Tunisia and surroundings from formal inversion of focal mechanisms: geodynamic implications for central Mediterranean. Tectonics 34: 1154-1180. doi: 10.1002/2015tc003895

Tseng T-L, Hsu H-C, Jian P-R, Huang B-S, Hu J-C et al. (2016). Focal mechanisms and stress variations in the Caucasus and northeast Turkey from constraints of regional waveforms. Tectonophysics 691: 362-374. doi: 10.1016/j.tecto.2016.10.028

Wallace RE (1951). Geometry of shearing stress and relation to faulting. The Journal of Geology 59: 118-130. doi: 10.1086/625831

Appendix

date	time	lat	long	depth(km)	strike1	dip1	rake1	reference	Mw	Mb	Ms	Mn	Ml
1931.04.07		39,48	46,09		135	90	180	Jackson et al., 1995			6,4		
1935.05.01		40,5	43,3		115	74	180	Jackson et al., 1995			6,2		
1952.01.03		39,9	41,6		102	90	180	Jackson et al., 1995			6		
1964.06.05	00.11.51	39,13	43,19	42	229	49	35	Mostriouk and Petrov, 1994		4,6			
1965.02.10	16.09.54	37,66	47,09	45	192	23	-16	Mostriouk and Petrov, 1994		5			
1966.03.07	01.16.08	39,2	41,6	26	208	65	-9	Mostriouk and Petrov, 1994		5,2			
1966.08.09		39,17	41,56		304	64	163	Jackson et al., 1995			6,8		
1966.08.19	12.22.10	39,17	41,56	0	39	56	53	Mostriouk and Petrov, 1994		5,8			
1966.08.19	13.54.25	38,99	41,77	32	235	62	-4	Mostriouk and Petrov, 1994		5,2			
1967.01.30	12.25.04	39,41	41,49	76	150	53	-30	Mostriouk and Petrov, 1994		4,6			
1968.04.29	17.01.55	39,24	44,23	17	197	56	-18	Mostriouk and Petrov, 1994		5,3			
1968.06.09	00.56.32	39,09	46,1	31	207	82	-9	Mostriouk and Petrov, 1994		5			
1968.09.01	05.39.45	39,14	46,2	24	253	30	-4	Mostriouk and Petrov, 1994		5			
1970.02.17	02.59.56	38,65	43,36	47	202	86	-18	Mostriouk and Petrov, 1994		4,7			
1970.03.14	01.51.47	38,62	44,8	50	253	64	-6	Mostriouk and Petrov, 1994		5,2			
1972.07.16	02.46.51	38,23	43,36	46	323	71	-20	Mostriouk and Petrov, 1994		4,9			
1976.01.12	22.41.51	38,61	43,2	56	255	39	28	Mostriouk and Petrov, 1994		4,9			
1976.04.02	16.58.04	39,85	43,69	15	204	48	-49	Mostriouk and Petrov, 1994		4,6			
1976.11.24	12.22.25	39,12	44,03		115	74	180	Jackson et al., 1995	7,2				
1976.11.24	13.18.08	39,09	43,71	49	197	48	-10	Mostriouk and Petrov, 1994		4,9			
1976.11.24	15.04.05	39,18	43,71	46	124	55	135	Mostriouk and Petrov, 1994		4,9			
1976.11.24	20.46.07	39,08	44,13	55	230	51	-3	Mostriouk and Petrov, 1994		4,9			
1976.11.24	15.11.07	39	44,19	62	172	57	-29	Mostriouk and Petrov, 1994		5			
1976.11.24	12.36.48	39,1	44,2	63	250	56	12	Mostriouk and Petrov, 1994		5,5			
1976.11.25	09.49.26	38,96	44,28	38	251	57	-71	Mostriouk and Petrov, 1994		5			
1976.12.04	04.10.36	39,31	43,66	53	300	37	-113	Mostriouk and Petrov, 1994		4,9			
1976.12.12	07.54.20	39	44,26	41	225	73	-33	Mostriouk and Petrov, 1994		4,8			
1977.01.02	19.37.26	39,29	43,62	46	220	47	-56	Mostriouk and Petrov, 1994		4,9			
1977.01.17	05.19.24	39,27	43,7	40	195	50	-24	Mostriouk and Petrov, 1994		5			
1977.05.26	09.50.24	38,89	44,35	41	255	61	-8	Mostriouk and Petrov, 1994		4,9			
1977.05.26	01.35.13	38,92	44,38	38	224	56	19	Mostriouk and Petrov, 1994		5,2			
1977.11.03	19.46.16	39,31	43,53	38	50	86	45	Mostriouk and Petrov, 1994		4,9			
1979.04.11	12.14.27	39,12	43,91	44	49	65	73	Mostriouk and Petrov, 1994		4,9			

date	time	lat	long	depth(km)	strike1	dip1	rake1	reference	Mw	Mb	Ms	Mn	Ml
1980.10.10	11.09.53	38,4	45,91	47	293	76	-30	Mostriouk and Petrov, 1994		4,8			
1980.12.11	00.14.36	40,31	46,07	18	148	61	145	Mostriouk and Petrov, 1994		4,8			
1981.01.04	07.19.46	38,48	44,91	38	28	73	64	Mostriouk and Petrov, 1994		4,6			
1982.03.27	19.57.24	39,23	41,9	38	172	51	-8	Mostriouk and Petrov, 1994		5,4			
1982.05.19	13.32.58	40,06	42,26	62	231	28	-120	Mostriouk and Petrov, 1994		4,7			
1982.05.29	14.22.01	39,4	43,72	33	77	74	168	Mostriouk and Petrov, 1994		4,8			
1982.10.13	03.51.31	39,19	41,92	41	27	53	124	Mostriouk and Petrov, 1994		4,7			
1983.12.15	07.17.42	40,24	46,11	5	259	7	91	Mostriouk and Petrov, 1994		4,4			
1984.06.29	19.55.18	38,42	45,16	40	262	5	15	Mostriouk and Petrov, 1994		4,6			
1985.11.07	08.26.18	39,75	41,68	10	233	58	22	CMT	5,2				
1986.01.01	06.09.06	39,13	41,83	36	88	86	106	Mostriouk and Petrov, 1994		4,8			
1986.04.11	04.10.34	40,01	43,34	33	201	52	-48	Mostriouk and Petrov, 1994		4,9			
1986.07.12	17.00.54	38,4	45,15	45	333	50	122	Mostriouk and Petrov, 1994		4,8			
1986.08.10	17.47.57	38,48	43,43	53	279	69	-79	Mostriouk and Petrov, 1994		4,7			
1988.01.27	03.47.00	39,84	45,12	36	30	49	45	Mostriouk and Petrov, 1994		4,7			
1988.04.20	03.50.08	39,11	44,12	48	229	33	8	Mostriouk and Petrov, 1994		5,1			
1988.04.21	10.01.48	39,09	44,1	40	248	59	-19	Mostriouk and Petrov, 1994		4,6			
1988.06.25	16.15.38	38,5	43,07	49	189	51	-33	Mostriouk and Petrov, 1994		5,3			
1988.12.07	09.34.34	40,93	44,08	8	22	56	33	Mostriouk and Petrov, 1994		5			
1988.12.07	07.41.24	40,96	44,16	5	44	74	57	Mostriouk and Petrov, 1994		6			
1988.12.07	18.05.42	40,9	44,21	2	79	84	89	Mostriouk and Petrov, 1994		4,4			
1988.12.07	08.06.29	40,83	44,23	16	165	86	-39	Mostriouk and Petrov, 1994		4,7			
1988.12.08	07.46.03	40,91	44,42	22	10	51	-40	Mostriouk and Petrov, 1994		4,8			
1988.12.31	04.07.09	40,95	44,05	2	72	78	98	Mostriouk and Petrov, 1994		4,7			
1989.01.04	07.29.40	40,93	44,26	3	18	89	78	Mostriouk and Petrov, 1994		4,9			
1989.12.02	04.51.59	38,45	45,42	20	175	65	75	Mostriouk and Petrov, 1994		4,5			
1989.12.03	07.39.12	38,44	45,35	40	290	6	-2	Mostriouk and Petrov, 1994		4,8			
1990.05.27	18.27.58	40,92	44,24	14	16	51	81	Mostriouk and Petrov, 1994		4,9			
1990.12.16	15.45.35	40,53	43,18	17,6	239	81	-1	CMT	5,4				
1991.03.27	22.17.54	40,43	45,43	26	53	56	55	Mostriouk and Petrov, 1994		4,3			
1991.06.03	10.22.41	40,07	42,85	34	264	67	-6	Mostriouk and Petrov, 1994		5			
1991.06.16	11.07.12	40,1	42,97	29	225	24	37	Mostriouk and Petrov, 1994		4,5			
1997.02.28	12,57	38,1	47,49	9	183	81	-1	Jackson et al., 2002	6				

date	time	lat	long	depth(km)	strike1	dip1	rake1	reference	Mw	Mb	Ms	Mn	Ml
1997.03.02	18.29.45	37,86	47,87	15	200	41	2	CMT	5,3				
2000.11.15	15.05.37	38,35	42,93	18	217	20	37	Bernardi et al., 2004	5,6				
2000.11.15	16,06	38,48	42,89	18	76	56	113	Pınar et al., 2007	4,5				
2000.11.15	16,43	38,45	42,91	15	85	75	130	Pınar et al., 2007	3,9				
2000.11.15	17,07	38,46	42,94	12	114	43	142	Pınar et al., 2007	3,5				
2000.11.15	17,44	38,48	42,94	15	89	50	110	Pınar et al., 2007	3,5				
2000.11.15	18,16	38,48	42,92	15	90	59	127	Pınar et al., 2007	3,8				
2000.11.15	19,3	38,42	42,87	15	109	63	130	Pınar et al., 2007	4,3				
2000.11.15	21,17	38,46	42,94	15	49	42	104	Pınar et al., 2007	3,6				
2000.11.16	21,13	38,41	42,89	15	73	55	129	Pınar et al., 2007	4,1				
2000.11.17	0,27	38,42	42,9	15	109	55	124	Pınar et al., 2007	4,3				
2000.11.17	9,36	38,39	42,92	15	117	46	136	Pınar et al., 2007	3,5				
2000.11.19	0,02	38,24	42,86	15	131	65	149	Pınar et al., 2007	3,7				
2000.11.25	0,59	38,28	42,86	15	125	64	147	Pınar et al., 2007	3,5				
2000.11.25	1,19	38,27	42,86	15	130	68	157	Pınar et al., 2007	3,5				
2000.11.30	10,3	38,24	42,85	12	123	51	127	Pınar et al., 2007	3,4				
2001.05.29	13.14.30	39,8	41,65	21	19	88	10	ISC	4,9				
2001.05.29	14.15.54	39,84	41,96	24	98	51	137	ISC	4,9				
2001.06.12	01.46.49	39,02	47,26	15	97	47	110	ISC	4,5				
2001.07.10	21.42.06	39,88	41,59	31	284	71	-170	Bernardi et al., 2004	5,3				
2001.10.23	10.41.28	38,64	43,4	12	246	38	60	CMT	7,1				
2001.12.02	04.11.48	38,43	43,25	18	72	50	83	ISC	4,7				
2002.03.14	12.56.58	39,35	44,12	21	46	89	17	ISC	4,5				
2002.04.07	22.50.31	38,38	45,26	15	42	37	126	ISC	4,7				
2003.08.11	20.12.08	38,83	44,88	24	34	62	11	ISC	5				
2003.10.20	06.26.51	38,65	44,57	21	52	79	3	ISC	5,1				
2004.01.24	04.40.47	38,07	44,92	12	217	20	86	ISC	6				
2004.04.27	17.30.	38,67	46,77	21	195	70	14	Siahkali Moradi et al., 2011					
2004.05.01	23.40.34	38,15	45,9	17,26	255	41	132	Siahkali Moradi et al., 2009		1,4			
2004.05.01	23.40.	38,15	45,88	19	255	40	42	Siahkali Moradi et al., 2011					
2004.05.05	06.32.35	38	46,8	13,2	107	61	-171	Siahkali Moradi et al., 2009		2,8			
2004.05.05	06.23.	37,99	46,81	12	350	45	-27	Siahkali Moradi et al., 2011					
2004.05.05	06.32.	37,99	46,8	14	340	70	-53	Siahkali Moradi et al., 2011					

date	time	lat	long	depth(km)	strike1	dip1	rake1	reference	Mw	Mb	Ms	Mn	Ml
2004.05.05	08.06.	37,99	46,8	7	100	30	-107	Siahkali Moradi et al., 2011					
2004.05.07	00.11.42	38,44	45,64	7,9	287	63	82	Siahkali Moradi et al., 2009				2,9	
2004.05.07	17.58.30	38,44	45,65	18,21	288	51	164	Siahkali Moradi et al., 2009				2,5	
2004.05.07	20.22.43	37,88	46,94	16,31	189	73	25	Siahkali Moradi et al., 2009				2	
2004.05.07	00.11.	38,44	45,61	18	105	70	165	Siahkali Moradi et al., 2011					
2004.05.07	17.58.	38,43	45,6	17	300	60	160	Siahkali Moradi et al., 2011					
2004.05.07	20.22.	37,87	46,94	15	200	60	19	Siahkali Moradi et al., 2011					
2004.05.18	11,29	38,43	45,27	16	340	60	-19	Siahkali Moradi et al., 2011					
2004.05.23	21,27	38,13	46,33	20	250	70	133	Siahkali Moradi et al., 2011					
2004.05.24	03.16.	38,48	46,47	21	210	80	-26	Siahkali Moradi et al., 2011					
2004.05.29	05.52.	38,13	46,44	5	90	80	-153	Siahkali Moradi et al., 2011					
2004.06.01	23,13	37,92	46,63	12	90	70	165	Siahkali Moradi et al., 2011					
2004.06.04	13,15	37,87	46,96	5	115	80	-153	Siahkali Moradi et al., 2011					
2004.06.14	22,54	38,26	46,03	11	100	70	-152	Siahkali Moradi et al., 2011					
2004.06.21	21.49.52	38,14	46,43	17	293	60	145	Siahkali Moradi et al., 2009		1,7			
2004.06.22	23.39.41	38,15	46,38	13,9	294	86	170	Siahkali Moradi et al., 2009				1,3	
2004.06.25	15,31	38,06	46,25	16	265	70	165	Siahkali Moradi et al., 2011					
2004.07.01	22.30.13	39,65	43,83	13,2	300	50	152	CMT	5,1				
2004.07.07	07.25.	38,11	46,38	5	120	80	134	Siahkali Moradi et al., 2011					
2004.07.08	11.21.20	38,37	45,76	15,9	280	60	149	Siahkali Moradi et al., 2009				2	
2004.07.09	09.09.	37,95	46,64	6	90	75	161	Siahkali Moradi et al., 2011					
2004.07.09	00.17.	38,15	46,9	4	210	75	34	Siahkali Moradi et al., 2011					
2004.07.09	00.19.	38,11	46,88	20	270	80	90	Siahkali Moradi et al., 2011					
2004.07.10	21.17.24	37,92	46,62	7,5	100	75	-180	Siahkali Moradi et al., 2009				1,3	
2004.07.13	02.26.13	38,34	45,67	18,32	266	59	60	Siahkali Moradi et al., 2009				2,7	
2004.07.13	02.26.	38,36	45,66	14	290	70	-152	Siahkali Moradi et al., 2011					
2004.07.20	09.53.	38,05	46,86	13	340	50	90	Siahkali Moradi et al., 2011					
2004.07.30	07.14.07	39,63	43,97	24	31	82	-8	ISC	4,9				
2004.09.26	21.03.14	38,61	43,31	15	88	41	94	ISC	4,5				
2005.03.13		40,19	45,52	10	278	60	-55	Lukk and Shevchenko, 2019		4,5			
2007.01.21	07.39.02	39,6	42,72	14,7	302	78	-177	CMT	5,1				
2008.04.29	05.20.38	40,29	45,96	12	124	89	121	Tseng et al., 2016	3,6				
2008.09.02	20.00.54	38,69	45,79	15,4	113	80	-179	CMT	5				

date	time	lat	long	depth(km)	strike1	dip1	rake1	reference	Mw	Mb	Ms	Mn	Ml
2009.07.25	20.06.39	40,08	43,2	13	241	32	46	Tseng et al., 2016	3,8				
2011.09.03	00.30.51	37,55	47,82	7,5	154	90	169	Ansari et al., 2015	4				4
2011.10.23	20.45.34	38,63	43,08	5	248	71	90	Irmak et al., 2012					5,7
2011.10.23	10,48	38,75	43,59	10	47	51	107	Kalafat et al., 2013	5,6				
2011.10.23	10,56	38,82	43,42	12	221	34	123	Kalafat et al., 2013	5,5				
2011.10.23	11.32.41	38,81	43,3	15	255	60	90	Gorgun, 2013	6,1				
2011.10.23	18.53.48	38,41	43,34	5	219	57	25	Irmak et al., 2012					4,9
2011.10.23	19.06.06	38,79	43,3	5	228	64	-90	Irmak et al., 2012					4,9
2011.10.24	15,28	38,69	43,17	5	252	44	49	Kalafat et al., 2013	4,8				
2011.10.24	06.46.41	38,8	43,62	15	195	90	0	Gorgun, 2013	4,4				
2011.10.24	20.15.49	38,88	43,47	5	259	56	36	Irmak et al., 2012					3,6
2011.10.24	16.24.19	38,92	43,51	3,7	289	56	43	Irmak et al., 2012					3,6
2011.10.25	00.32.17	38,5	43,3	5	270	45	30	Gorgun, 2013	4,3				
2011.10.25	15.05.25	38,79	43,49	14	60	90	0	Gorgun, 2013	4,5				
2011.10.25	16.56.18	38,59	43,51	15	75	90	165	Gorgun, 2013	4,5				
2011.10.25	14,55	38,79	43,54	8	264	53	68	Kalafat et al., 2013	5,4				
2011.10.25	03.28.51	38,84	43,67	2,2	283	57	43	Irmak et al., 2012					3,7
2011.10.25	00.16.40	38,55	43,11	5	126	74	-34	Irmak et al., 2012					3,7
2011.10.25	00.26.26	38,9	43,47	5	285	57	42	Irmak et al., 2012					3,6
2011.10.25	02.39.38	38,74	43,21	4	115	61	146	Irmak et al., 2012					3,5
2011.10.26	03.16.20	38,75	43,29	30,6	102	36	127	CMT	4,8				
2011.10.29	22.24.25	38,83	43,52	19,4	298	77	-172	CMT	5,1				
2011.10.29	18.45.49	38,7	43,1	20	180	90	-15	Gorgun, 2013	4,3				
2011.11.02	20.48.21	38,9	43,3	20	255	30	75	Gorgun, 2013	4,4				
2011.11.02	04.43.20	38,87	43,57	5	171	58	-61	Irmak et al., 2012					4,8
2011.11.06	02.43.16	38,82	43,5	15,8	277	64	-176	CMT	4,7				
2011.11.08	22,05	38,75	43,05	8	271	44	69	Kalafat et al., 2013	5,1				
2011.11.09	19.23.34	38,43	43,23	5,8	223	55	63	Irmak et al., 2012					5,6
2011.11.09	22.38.18	38,45	43,21	5	238	43	90	Irmak et al., 2012					4,5
2011.11.18	17,39	38,87	43,82	24	33	90	29	Kalafat et al., 2013	4,9				
2011.11.30	00.47.21	38,51	43,41	2,8	174	81	-32	Irmak et al., 2012					5
2011.12.03	01.30.55	38,8	43,5	5	60	75	30	Gorgun, 2013	4,5				
2011.12.04	22,15	38,47	43,29	28	209	82	6	Kalafat et al., 2013	4,7				

date	time	lat	long	depth(km)	strike1	dip1	rake1	reference	Mw	Mb	Ms	Mn	Ml
2012.12.23	06.38.58	38,49	44,93	11	70	68	149	Hosseini et al., 2019	5			4,9	
2012.01.06	0,16	38,74	43,55	32	114	78	13	Kalafat et al., 2013	4,5				
2012.01.20	9,57	38,94	43,69	5	238	61	99	Kalafat et al., 2013	4,4				
2012.01.21	00.45.00	39,92	41,71	18,4	44	82	54	ISC		3,4			
2012.01.29	4,14	38,98	43,38	14	91	87	-24	Kalafat et al., 2013	4,6				
2012.01.29	9,59	39,03	43,62	5	235	75	44	Kalafat et al., 2013	4				
2012.02.17	9,32	38,72	43,33	22	354	89	46	Kalafat et al., 2013	4,5				
2012.02.24	13,07	38,84	43,62	8	297	40	163	Kalafat et al., 2013	4,4				
2012.03.23	15,43	38,97	43,65	10	137	77	-140	Kalafat et al., 2013	4,2				
2012.03.24	6,57	38,94	43,52	8	63	67	21	Kalafat et al., 2013	4,3				
2012.03.26	10.35.35	39,15	42,2	19,5	82	44	94	CMT	5,2				
2012.03.31	10,38	39,08	43,81	20	355	46	-180	Kalafat et al., 2013	4				
2012.04.04	9,41	38,93	43,6	20	274	85	-166	Kalafat et al., 2013	4,4				
2012.04.13	0,04	39,04	44,09	12	40	84	-166	Kalafat et al., 2013	4,4				
2012.04.13	4,22	38,66	43,18	4	248	50	75	Kalafat et al., 2013	4,3				
2012.04.18	23,3	38,89	43,49	22	327	78	-115	Kalafat et al., 2013	4,6				
2012.06.24	20,07	38,55	43,52	8	294	55	116	Kalafat et al., 2013	5				
2012.07.20	16,2	38,67	43,37	6	72	60	83	Kalafat et al., 2013	5				
2012.07.24	22,53	38,71	43,14	14	115	78	-162	Kalafat et al., 2013	4,4				
2012.08.11	12.23.16	38,4	46,84	6	265	45	166	Donner et al., 2015	6,4				
2012.08.11	12.34.35	38,42	46,78	12	257	61	125	Donner et al., 2015	6,2				
2012.08.11	15.21.15	38,46	46,83	10	80	79	164	Donner et al., 2015	4,6				
2012.08.11	15.43.19	38,42	46,72	14	251	33	118	Donner et al., 2015	4,7				
2012.08.11	19.52.43	38,44	46,79	10	279	65	140	Donner et al., 2015	4,3				
2012.08.11	22.24.02	38,44	46,71	12	252	77	148	Donner et al., 2015	5,1				
2012.08.11	13.14.05	38,43	46,68	6	259	75	113	Donner et al., 2015	4,8				
2012.08.13	01.56.10	38,45	46,68	10	271	74	-173	Donner et al., 2015	4,4				
2012.08.14	14.02.26	38,51	46,78	12	274	89	162	Donner et al., 2015	4,9				
2012.08.14	15.48.20	38,38	46,64	3,2	217	48	58	Momeni and Tatar, 2018					3,9
2012.08.14	12.33.18	38,42	46,73	10,8	8	77	52	Momeni and Tatar, 2018					3,2
2012.08.14	20.10.56	38,38	46,77	10,8	31	56	88	Momeni and Tatar, 2018					3,4
2012.08.15	17.49.05	38,44	46,67	8	214	55	87	Donner et al., 2015	5				
2012.08.15	16.28.54	38,37	46,76	11,8	356	77	7	Momeni and Tatar, 2018					3,2

date	time	lat	long	depth(km)	strike1	dip1	rake1	reference	Mw	Mb	Ms	Mn	Ml
2012.08.15	13.34.33	38,4	46,76	11,3	201	50	-23	Momeni and Tatar, 2018					3,2
2012.08.16	17.14.13	38,46	46,73	12	271	82	149	Donner et al., 2015	4,8				
2012.08.16	04.39.47	38,39	46,62	5,9	49	56	70	Momeni and Tatar, 2018					3,3
2012.08.16	19.48.46	38,42	46,7	12,3	12	80	47	Momeni and Tatar, 2018					3
2012.08.16	16.59.08	38,42	46,71	11,8	5	61	28	Momeni and Tatar, 2018					3
2012.08.16	21.00.22	38,42	46,71	11	15	72	55	Momeni and Tatar, 2018					3,4
2012.08.16	15.15.35	38,43	46,71	12,2	257	76	153	Momeni and Tatar, 2018					4,1
2012.08.16	05.05.03	38,38	46,78	8,1	224	32	82	Momeni and Tatar, 2018					3
2012.08.17	19.34.08	38,41	46,59	4,4	166	87	-48	Momeni and Tatar, 2018					3,2
2012.08.17	03.34.20	38,39	46,66	4,2	230	44	64	Momeni and Tatar, 2018					3,1
2012.08.17	04.48.15	38,38	46,67	4,5	345	37	44	Momeni and Tatar, 2018					3,8
2012.08.17	08.09.51	38,39	46,86	5	202	84	-46	Momeni and Tatar, 2018					3,6
2012.08.18	05.45.22	38,42	46,7	13,2	11	55	33	Momeni and Tatar, 2018					3,7
2012.08.18	13.20.29	38,39	46,79	9,7	44	45	79	Momeni and Tatar, 2018					3,1
2012.08.19	11.37.16	38,38	46,62	5,7	220	43	72	Momeni and Tatar, 2018					4,1
2012.08.19	01.58.30	38,38	46,63	5,9	197	57	61	Momeni and Tatar, 2018					4
2012.08.20	08.49.37	38,42	46,69	12,4	0	64	21	Momeni and Tatar, 2018					3,1
2012.08.20	08.48.17	38,42	46,69	12,9	10	76	30	Momeni and Tatar, 2018					3,4
2012.08.20	13.47.33	38,42	46,7	12,3	5	63	37	Momeni and Tatar, 2018					3
2012.08.21	06.48.23	38,41	46,77	13,5	35	60	31	Momeni and Tatar, 2018					3
2012.08.22	19.44.59	38,39	46,62	5,5	222	61	78	Momeni and Tatar, 2018					3,1
2012.08.22	02.35.47	38,37	46,65	4,9	36	39	65	Momeni and Tatar, 2018					3,4
2012.08.22	03.45.27	38,42	46,7	13	9	65	22	Momeni and Tatar, 2018					3
2012.08.22	05.28.35	38,42	46,7	12,4	8	63	19	Momeni and Tatar, 2018					4,3
2012.08.23	12.14.46	38,39	46,63	4,1	22	80	48	Momeni and Tatar, 2018					3
2012.08.23	15.01.08	38,42	46,79	12,9	35	52	87	Momeni and Tatar, 2018					3
2012.08.24	16.22.54	38,41	46,67	12,8	15	53	43	Momeni and Tatar, 2018					3,4
2012.08.25	21.52.12	38,38	46,65	5,9	340	34	-7	Momeni and Tatar, 2018					3,2
2012.08.25	19.29.40	38,43	46,79	11,5	26	82	50	Momeni and Tatar, 2018					3
2012.08.25	09.27.25	38,37	46,91	6	13	72	-8	Momeni and Tatar, 2018					3,3
2012.08.25	02.56.45	38,37	46,92	6,5	13	57	13	Momeni and Tatar, 2018					3
2012.08.26	13.08.36	38,38	46,65	5,5	31	62	67	Momeni and Tatar, 2018					3,5
2012.08.26	16.46.41	38,41	46,75	11,3	195	40	27	Momeni and Tatar, 2018					3,2

date	time	lat	long	depth(km)	strike1	dip1	rake1	reference	Mw	Mb	Ms	Mn	Ml
2012.08.26	05.27.49	38,41	46,78	11,8	9	53	39	Momeni and Tatar, 2018					3
2012.08.27	01.16.54	38,4	46,81	9,7	2	44	49	Momeni and Tatar, 2018					3
2012.08.27	23.56.31	38,4	46,87	9,1	7	78	-9	Momeni and Tatar, 2018					3,5
2012.08.28	17.58.52	38,39	46,63	5,8	196	67	48	Momeni and Tatar, 2018					3,7
2012.08.30	06.25.50	38,38	46,67	5,9	77	25	128	Momeni and Tatar, 2018					3
2012.08.31	20.35.56	38,38	46,67	6,1	173	54	4	Momeni and Tatar, 2018					3,6
2012.08.31	08.34.03	38,38	46,69	12,9	179	79	51	Momeni and Tatar, 2018					4,2
2012.09.01	05.04.04	38,38	46,76	9	54	62	85	Momeni and Tatar, 2018					3,8
2012.09.02	04.11.26	38,39	46,73	12,9	222	44	65	Momeni and Tatar, 2018					3,3
2012.09.02	08.50.11	38,4	46,75	9,2	325	86	30	Momeni and Tatar, 2018					4,1
2012.09.02	09.03.17	38,4	46,75	8,8	175	65	37	Momeni and Tatar, 2018					3,6
2012.09.23	09.10.	38,71	42,94	6	116	86	-60	Kalafat et al., 2013	4,5				
2012.10.08	08.25.54	38,45	46,63	4	353	45	36	Nemati, 2013				4,1	
2012.10.16	07.10.00	38,45	46,59	4	11	31	17	Nemati, 2013				4,1	
2012.10.26	22.31.15	38,46	46,65	10	162	86	46	Nemati, 2013				4,3	
2012.10.27	03.56.41	38,39	46,64	8	83	71	166	Afra et al., 2017	4,3				
2012.11.07	06.26.31	38,45	46,6	4	9	89	51	Donner et al., 2015	5,6				
2012.11.08	09.43.59	38,41	46,57	10	347	88	48	Nemati, 2013				4,2	
2012.11.10	13.51.22	38,49	46,62	4	212	59	16	Nemati, 2013				4	
2012.11.16	03.58.25	38,47	46,59	6	39	20	35	Donner et al., 2015	5				
2012.12.23	07.12.31	38,41	44,84	20	83	61	147	Afra et al., 2017	4,1				
2012.12.23	06.38.57	38,48	44,93	14	76	82	174	Afra et al., 2017	5,2				
2013.01.26	15.10.49	38,36	46,84	9	9	72	37	Hosseini et al., 2019	4,9			4,6	
2013.04.18	10.39.38	38,43	45,36	7	204	83	28	Hosseini et al., 2019	4,9				
2013.11.08	10.12.34	37,81	47,17	6	311	79	-173	Hosseini et al., 2019	4,4				
2013.03.03	20.50.03	38,4	46,68	6,4	4	48	31	Nemati, 2013				4,1	
2013.03.08	13.45.42	38,37	46,68	4	49	49	46	Nemati, 2013				4	
2013.06.12	19.02.55	38,52	43,62	10	290	48	178	GEOFON	4,5				
2013.09.18	18.22.40	39,69	41,65	9	46	70	-162	ISC	5,6				
2013.11.22	03.29.19	38,59	43,34	10	93	38	100	ISC	4,4				
201510.29	09.46.40	39,1	43,78	20	120	66	162	Hosseini et al., 2019	4,8			4,7	
2015.01.21	13.53.03	38,24	42,85	22	285	89	-173	KANDILLI	4,5				
2015.04.11	22.01.05	39,32	42,16	11	58	65	48	KANDILLI	3,7				

date	time	lat	long	depth(km)	strike1	dip1	rake1	reference	Mw	Mb	Ms	Mn	Ml
2015.04.28	14.01.01	38,9	43,58	23	309	78	166	KANDILLI	4,1				
2015.06.23	22.35.21	38,58	43,15	22,2	87	44	82	CMT	4,8				
2016.06.22	16.56.58	38,5	44,85	9	304	88	-166	Hosseini et al., 2019	4,3			4,3	
2016.01.07	02.01.45	38,9	43,53	22	198	89	2	KANDILLI	4,5				
2016.03.24	51.35.09	37,29	47,15	18,9	317	55	-30	SoleymaniAzad et al., 2019				4,2	
2016.11.23	12.14.23	38,53	43,82	4	24	87	6	ISC	4,4				
2016.12.12	22.42.08	38,51	43,83	5	45	80	29	KANDILLI	4,2				
2017.02.10	12.27.30	39,78	42,52	8	132	80	-179	KANDILLI	4,2				
2017.05.01	16.30.40	38,27	42,92	20	312	72	-170	KANDILLI	4,4				
2017.08.27	23.14.52	37,87	47,14	17,5	116	72	-177	CMT	5				
2018.06.23	03.50.02	38,53	44,34	9	113	61	133	KANDILLI	4,7				
2018.07.21	06.25.14	39,05	44,09	12	115	67	36	KANDILLI	4,6				
2019.11.07	22.47.05	37,81	47,56	10	311	75	-168	USGS	6				